Feedforward Transient Control for In-motion Wireless Power Transfer using Envelope Model

Keiichiro Tokita, Kensuke Hanajiri, Katsuhiro Hata, Takehiro Imura, Hiroshi Fujimoto and Yoichi Hori
The University of Tokyo
5-1-5, Kashiwanoha, Kashiwa, Chiba, 277-8561 Japan
tokita.keiichiro18@ae.k.u-tokyo.ac.jp

***Abstract*—In in-motion wireless power transfer (WPT) application, large current overshoot comes into being if the power transmission starts suddenly. For the safety of the equipment, the transient property when the power transmission starts needs to be improved. However, few studies have proposed transient control using accurate circuit models. In this paper, precise envelope modeling of circuit considering the discontinuous current mode of diodes is introduced for transient control. Besides, its application to the voltage trajectory generation with offline calculation is also proposed. The experimental results demonstrate that the proposed method can track reference current trajectory and eliminate the overshoot.**

***Index Terms*—wireless power transfer, in-motion charging, transient property, control, envelope model, constant voltage load**

I. Introduction

In recent years, wireless power transfer (WPT) has been widely studied. In particular, WPT using magnetic resonance coupling enables high-efficiency and high-power transmission even with a large air gap between a transmitting coil and a receiving coil [1], [2]. Therefore, it is expected to be used for many applications such as mobile devices, industrial machinery and transportation [3].

As a solution to environment problems and lack of fossil fuels, the use of electric vehicles (EVs) is expected to increase instead of gasoline-powered vehicles in future. However, current EVs have a serious problem in their shorter mileage per charge compared to gasoline-powered vehicles.

As a technique to use WPT for EVs, in-motion wireless power transfer has been studied [4], [5]. This is a method of transmitting power wirelessly from the transmitting coil on roads to the receiving coil on the bottom of EVs. The authors have developed in-motion WPT with the experimental electric vehicle in Fig. 1. This technique will not only solve the problem of short mileage per charge, but also enable large reduction of on-board batteries and price down of EVs.

However, in-motion WPT has unique problems which do not matter in previous WPT applications. When power is transmitted suddenly, a large overshoot comes into being in the transmitting-side and receiving-side current due to transient response. In order to protect equipment from the large current, the current overshoot must be decreased. For the practical use of in-motion WPT, it is important to improve the characteristics of transient response when the transmission starts [6], [7].

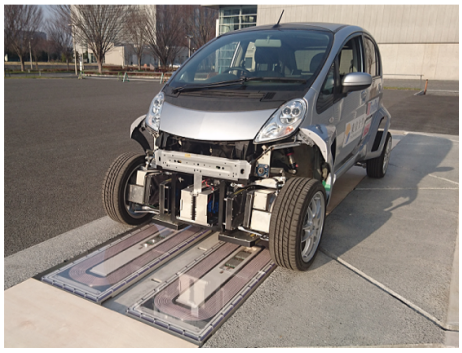

Fig. 1. Experimental electric vehicle FPEV4-Sawyer in our group.

For the control of transient response, previous studies have proposed modeling of transient response in different circuit topologies [8], [9]. However, these studies suppose the load as a pure resistance. This assumption makes analyses easy, but it is not appropriate for representing a circuit model of in-motion WPT. In the in-motion WPT circuit, a battery is connected to the receiving coil through a diode rectifier. Because the load keeps the receiving-side voltage constant when the diode conducts, it is called a Constant Voltage Load (CVL). CVL has a non-linear relation between voltage and current, so it cannot be precisely analyzed with a pure resistance. On the other hand, [10] proposes a precise envelope model of transient response of the WPT circuit with a CVL.

The modeling in [10] considers only the condition that the receiving-side current is high enough and the diode rectifier works. However, discontinuous current mode of diodes has to be considered because voltage and current are raised from zero when power transmission starts. In this paper, a control method of decreasing the overshoot is proposed by applying the envelope model [10] to the discontinuous current mode of diodes. Finally, the feasibility of proposed control method is verified by experiments.

II. Envelope Modeling

A. WPT circuit and concept of envelope model

Because high frequency AC is used in WPT via magnetic resonance coupling, it is difficult to control waveform of instantaneous current or voltage values. On the other hand, it is easier to control the envelope waveform because it does not

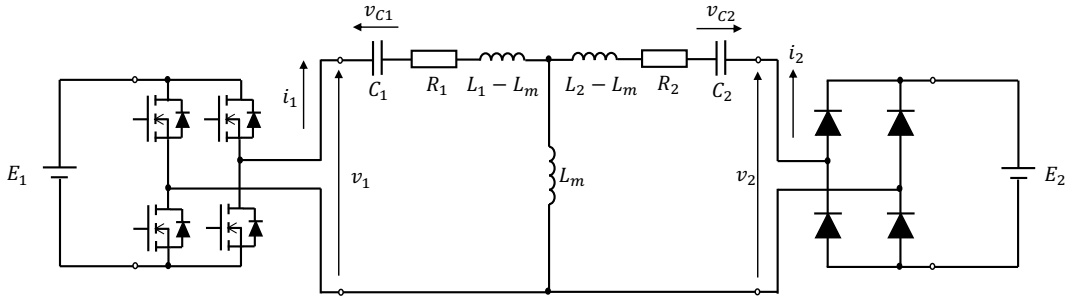

Fig. 2. WPT circuit with a CVL on the receiving side.

change as quickly as the instantaneous values. In this section, the envelope modeling is derived which describes the relation between the voltage and the envelope of current.

As shown in Fig. 2, the equivalent circuit which has the CVL on the receiving side is supposed to express in-motion WPT circuit. Both the transmitting side and the receiving side adopt LC series circuits (S-S compensation circuit). E_1 is DC source voltage, and high-frequency AC voltage on the transmitting side v_1 is made by the inverter. In this paper, every AC wave is regarded as a purely sinusoidal waveform and higher harmonics is neglected unless otherwise mentioned. This approximation is valid because the WPT circuit via magnetic resonance has band-pass property and higher harmonics are not associated to power transfer. L_1 and R_1 are self inductance and equivalent series resistance (ESR) of the transmitting coil, respectively. L_2 and R_2 are those of the receiving coil. L_m is the mutual inductance between the transmitting coil and the receiving coil and it has a relation with the coupling coefficient k as follows :

$$k = \frac{L_m}{\sqrt{L_1 L_2}}. \tag{1}$$

C_1 is capacitance for LC resonance of the transmitting side and C_2 is that of the receiving side. The receiving-side AC voltage v_2 is rectified by the diode rectifier and connected to the battery. E_2 is the battery voltage.

In the modeling, a sinusoidal wave is expressed as a phasor, as shown in (2).

$$\begin{aligned} f(t) &= A \cdot \cos(\omega \cdot t + \phi) \\ &= \mathrm{Re}(A \cdot e^{j\phi} \cdot e^{j\omega t}) \\ &= \mathrm{Re}\{(a + jb) \cdot e^{j\omega t}\} \\ &\equiv a + jb. \end{aligned} \tag{2}$$

This conversion enables us to express AC functions like current or voltage in the cartesian coordinates of d-axis and q-axis. For example, the sinusoidal wave of the transmitting-side current $i_1(t)$ is separated into the combination of two functions on the gauss plane, like

$$i_1(t) \equiv i_{1,d}(t) + j i_{1,q}(t). \tag{3}$$

From the definition of (2) and (3), both $i_{1,d}(t)$ and $i_{1,q}(t)$ become constants in the steady state, which is the state that the amplitude $|i_1(t)|$ is a constant.

Derivative of

$$x(t) \equiv x_d(t) + j x_q(t) \tag{4}$$

is necessary for state space model, and derived as follows :

$$\begin{aligned} \dot{x}(t) &= \mathrm{Re}\left[\frac{d}{dt}\{(x_d(t) + j x_q(t)) \cdot e^{j\omega t}\}\right] \\ &= \mathrm{Re}\left[(\dot{x_d}(t) + j\dot{x_q}(t)) \cdot e^{j\omega t} + (x_d(t) + j x_q(t)) \cdot j\omega \cdot e^{j\omega t}\right] \\ &= \mathrm{Re}\left[\{(\dot{x_d}(t) - \omega \cdot x_q(t)) + j(\dot{x_q}(t) + \omega \cdot x_d(t))\} \cdot e^{j\omega t}\right] \\ &\equiv (\dot{x_d}(t) - \omega \cdot x_q(t)) + j(\dot{x_q}(t) + \omega \cdot x_d(t)) \end{aligned} \tag{5}$$

The circuit equations of Fig. 2 are expressed as simultaneous equations with 4 variables : transmitting-side current i_1, receiving-side current i_2, transmitting-side capacitor voltage v_{C1} and receiving-side capacitor voltage v_{C2}. In this section, these four variables are expressed as phasors and state equations with 8 state variables are derived as follows :

$$\boldsymbol{x} = [i_{1d} \;\; i_{1q} \;\; i_{2d} \;\; i_{2q} \;\; v_{C1d} \;\; v_{C1q} \;\; v_{C2d} \;\; v_{C2q}]^T. \tag{6}$$

Now, $v_{2,act}(t)$ is defined as the actual value of receiving-side voltage including higher harmonics. According to the value, this circuit has two types of modes :

1) The absolute value of the instantaneous value of receiving-side AC voltage $|v_{2,act}(t)|$ is always lower than the battery voltage E_2, and the receiving-side rectifier does not conduct at all.
2) The absolute value of the instantaneous value of receiving-side AC voltage $|v_{2,act}(t)|$ reaches the battery voltage E_2, and the receiving-side rectifier conducts on and off.

The mode 1) is discussed in section II-B and the mode 2) in section II-C.

B. State equations when the rectifier does not conduct

When the absolute value of the instantaneous value of receiving-side AC voltage $|v_{2,act}(t)|$ is always lower than the battery voltage E_2 ($|v_{2,act}(t)| < E_2$), the receiving-side rectifier does not conduct and the receiving side is open. Then,

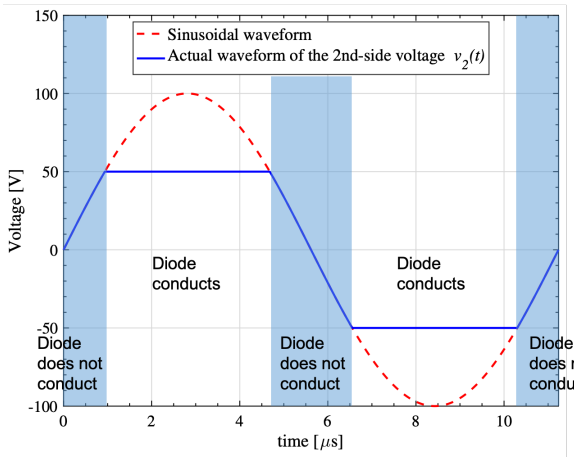

Fig. 3. Waveform of the receiving-side voltage $v_{2,act}(t)$ when the full bridge diodes work as a rectifier.

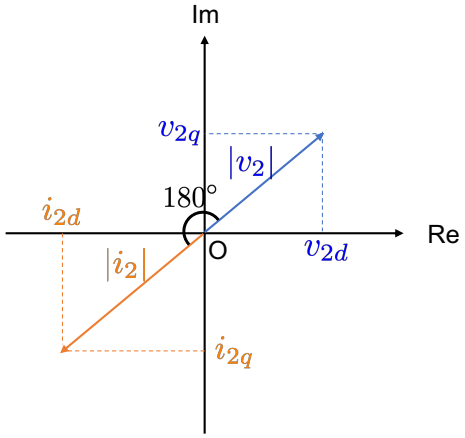

Fig. 4. The phase relation between v_2 and i_2.

the circuit equations are expressed as simultaneous equations with 4 variables :

$$L_1\frac{di_1}{dt} = -R_1 i_1 - v_{C1} + v_1 \tag{7}$$
$$C_1\frac{dv_{C1}}{dt} = i_1 \tag{8}$$
$$i_2 = 0 \tag{9}$$
$$v_{C2} = 0. \tag{10}$$

The d-q conversion mentioned in section II-A is applied to transmitting-side current i_1, receiving-side current i_2, transmitting-side capacitor voltage v_{C1}, and receiving-side capacitor voltage v_{C2}. According to (7)-(10), state equations with 8 state variables are given as follows: (11)-(18).

$$\frac{di_{1d}}{dt} = -\frac{R_1}{L_1}i_{1d} + \omega\cdot i_{1q} - \frac{1}{L_1}v_{C1d} + \frac{1}{L_1}v_{1d} \tag{11}$$
$$\frac{di_{1q}}{dt} = -\omega\cdot i_{1d} - \frac{R_1}{L_1}i_{1q} - \frac{1}{L_1}v_{C1q} + \frac{1}{L_1}v_{1q} \tag{12}$$
$$\frac{dv_{C1d}}{dt} = \frac{1}{C_1}i_{1d} + \omega\cdot v_{C1q} \tag{13}$$
$$\frac{dv_{C1q}}{dt} = -\omega\cdot v_{C1d} + \frac{1}{C_1}i_{1q} \tag{14}$$
$$i_{2d} = 0 \tag{15}$$
$$i_{2q} = 0 \tag{16}$$
$$v_{C2d} = 0 \tag{17}$$
$$v_{C2q} = 0. \tag{18}$$

C. State equations when the rectifier conducts

When the absolute value of the instantaneous value of receiving-side AC voltage $|v_{2,act}(t)|$ reaches the battery voltage E_2 ($|v_{2,act}(t)| = E_2$), the receiving-side rectifier conducts and the absolute value of the instantaneous value of receiving-side AC voltage $|v_{2,act}(t)|$ is limited not to overcome the battery voltage E_2. In this condition, the waveform of $v_{2,act}(t)$ becomes the shape of blue line in Fig. 3. When $|v_{2,act}(t)|$ is lower than E_2, the waveform varies according to a sinusoidal wave (blue-background area in Fig. 3). However, the waveform is limited to $\pm E_2$ when $|v_{2,act}(t)|$ reaches E_2 (white-background area in Fig. 3). If the amplitude of sinusoidal wave (red line in Fig. 3) is very large, the waveform of $v_{2,act}(t)$ can be approximated by a rectangular wave.

Then, the circuit equations are as follows:

$$L_{\sigma1}\frac{di_1}{dt} = -R_1 i_1 + \frac{L_m R_2}{L_2}i_2 - v_{C1} + \frac{L_m}{L_2}v_{C2} + v_1 - \frac{L_m}{L_2}v_2 \tag{19}$$
$$L_{\sigma2}\frac{di_2}{dt} = \frac{L_m R_1}{L_1}i_1 - R_2 i_2 + \frac{L_m}{L_1}v_{C1} - v_{C2} - \frac{L_m}{L_1}v_1 + v_2 \tag{20}$$
$$C_1\frac{dv_{C1}}{dt} = i_1 \tag{21}$$
$$C_2\frac{dv_{C2}}{dt} = i_2. \tag{22}$$

$L_{\sigma1}$ and $L_{\sigma2}$ above are defined as follows:

$$L_{\sigma1} = L_1 - \frac{L_m^2}{L_2} \tag{23}$$
$$L_{\sigma2} = L_2 - \frac{L_m^2}{L_1} \tag{24}$$

The d-q conversion mentioned in section II-A is applied to (19)-(22) as well as section II-B. Constant Voltage Load (CVL) and a rectifier have two properties in the steady state as follows :

1) The phase difference between receiving-side voltage v_2 and receiving-side current i_2 is 180 degree (opposite phase).
2) The amplitude of receiving-side voltage $|v_2|$ is determined as a function of the amplitude of transmitting-side voltage $|v_1|$ and battery voltage E_2.

Due to the first property,

$$v_{2d} = -|v_2|\cdot\frac{i_{2d}}{\sqrt{i_{2d}^2 + i_{2q}^2}} \tag{25}$$
$$v_{2q} = -|v_2|\cdot\frac{i_{2q}}{\sqrt{i_{2d}^2 + i_{2q}^2}} \tag{26}$$

are derived because of the relation as shown in Fig. II-C. Then, $|v_2|$ should be solved due to the second property. By using Fourier series expansion to the waveform shown in Fig. 3, the amplitude of the fundamental wave at the operating frequency is calculated. As a consequence, $|v_2|$ is expressed as follows :

$$|v_2| = \frac{2X}{\pi}\sin^{-1}\left(\frac{E_2}{X}\right) + \frac{2E_2}{\pi}\sqrt{1-\left(\frac{E}{X}\right)^2}, \tag{27}$$

where X in (27) is the amplitude of the sinusoidal wave, and is defined as follows:

$$X = \frac{\omega L_m}{R_1}|v_1|. \tag{28}$$

By these two characters, v_{2d} and v_{2q} are expressed as a non-linear functions of state variables. Accordingly, (19)-(22) are expressed as state equations with 8 state variables as following (29)-(36).

$$\begin{aligned}\frac{di_{1d}}{dt} &= -\frac{R_1}{L_{\sigma 1}}i_{1d} + \omega \cdot i_{1q} + \frac{L_m R_2}{L_{\sigma 1}L_2}i_{2d} - \frac{1}{L_{\sigma 1}}v_{C1d} \\ &\quad + \frac{L_m}{L_{\sigma 1}L_2}v_{C2d} + \frac{1}{L_{\sigma 1}}v_{1d} + \frac{L_m|v_2|}{L_{\sigma 1}L_2}\frac{i_{2d}}{\sqrt{i_{2d}^2+i_{2q}^2}}\end{aligned} \tag{29}$$

$$\begin{aligned}\frac{di_{1q}}{dt} &= -\omega \cdot i_{1d} - \frac{R_1}{L_{\sigma 1}}i_{1q} + \frac{L_m R_2}{L_{\sigma 1}L_2}i_{2q} - \frac{1}{L_{\sigma 1}}v_{C1q} \\ &\quad + \frac{L_m}{L_{\sigma 1}L_2}v_{C2q} + \frac{1}{L_{\sigma 1}}v_{1q} + \frac{L_m|v_2|}{L_{\sigma 1}L_2}\frac{i_{2q}}{\sqrt{i_{2d}^2+i_{2q}^2}}\end{aligned} \tag{30}$$

$$\begin{aligned}\frac{di_{2d}}{dt} &= \frac{L_m R_1}{L_{\sigma 2}L_1}i_{1d} - \frac{R_2}{L_{\sigma 2}}i_{2d} + \omega \cdot i_{2q} + \frac{L_m}{L_{\sigma 2}L_1}v_{C1d} \\ &\quad - \frac{1}{L_{\sigma 2}}v_{C2d} - \frac{L_m}{L_{\sigma 2}L_1}v_{1d} - \frac{|v_2|}{L_{\sigma 2}}\frac{i_{2d}}{\sqrt{i_{2d}^2+i_{2q}^2}}\end{aligned} \tag{31}$$

$$\begin{aligned}\frac{di_{2q}}{dt} &= \frac{L_m R_1}{L_{\sigma 2}L_1}i_{1q} - \omega \cdot i_{2d} - \frac{R_2}{L_{\sigma 2}}i_{2q} + \frac{L_m}{L_{\sigma 2}L_1}v_{C1q} \\ &\quad - \frac{1}{L_{\sigma 2}}v_{C2q} - \frac{L_m}{L_{\sigma 2}L_1}v_{1q} - \frac{|v_2|}{L_{\sigma 2}}\frac{i_{2q}}{\sqrt{i_{2d}^2+i_{2q}^2}}\end{aligned} \tag{32}$$

$$\frac{dv_{C1d}}{dt} = \omega \cdot v_{C1q} + \frac{1}{C_1}i_{1d} \tag{33}$$

$$\frac{dv_{C1q}}{dt} = -\omega \cdot v_{C1d} + \frac{1}{C_1}i_{1q} \tag{34}$$

$$\frac{dv_{C2d}}{dt} = \omega \cdot v_{C2q} + \frac{1}{C_2}i_{2d} \tag{35}$$

$$\frac{dv_{C2q}}{dt} = -\omega \cdot v_{C2d} + \frac{1}{C_2}i_{2q}. \tag{36}$$

$|v_2|$ in (29)-(36) are defined as (27) and (28).

III. Trajectory Generation

A. Output equations of current envelope

In the section II, state eqtions in two cases were derived. Because the state equations include non-linear terms when the rectifier conducts, they can be regarded as a non-linear state equation as (37).

$$\dot{\boldsymbol{x}} = \boldsymbol{f}(\boldsymbol{x}, \boldsymbol{u}) \tag{37}$$

$\boldsymbol{x}$ is the state vector which consists of 8 state variables :

$$\boldsymbol{x} = [i_{1d} \;\; i_{1q} \;\; i_{2d} \;\; i_{2q} \;\; v_{C1d} \;\; v_{C1q} \;\; v_{C2d} \;\; v_{C2q}]^T \tag{38}$$

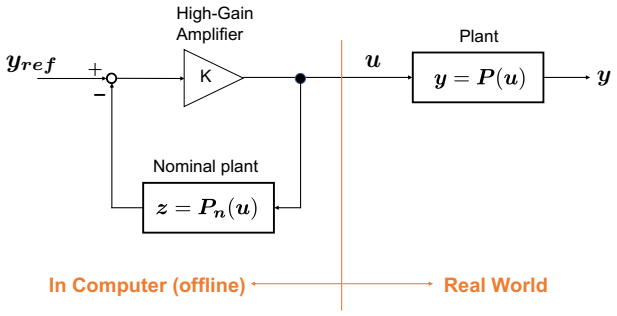

Fig. 5. Block diagram of high gain feedback.

and $\boldsymbol{u}$ is the input vector which consists of 2 input variables :

$$\boldsymbol{u} = [v_{1d} \;\; v_{1q}]^T \tag{39}$$

The conversion in section II-A has a degree of freedom in the direction of axes, so it is possible to choose it with reference to a certain variable. By determining the direction of axes so that the q component of transmitting-side voltage v_{1q} always equals 0, the system can be regarded as one-input system of the amplitude of transmitting-side voltage $|v_1|$:

$$\boldsymbol{u} = v_{1d} = |v_1|, \tag{40}$$

instead of (39).

Envelope of transmitting-side current is the norm of the phasor i_1, so it can be derived by the non-linear output equation (41).

$$\boldsymbol{y} = \boldsymbol{g}(\boldsymbol{x}) = \sqrt{i_{1d}^2 + i_{1q}^2} \tag{41}$$

In this paper, the trajectory of amplitude of transmitting-side voltage $\boldsymbol{u}(t)$ should be derived so that the envelope of transmitting-side current $\boldsymbol{y}(t)$ is the reference trajectory $\boldsymbol{y_{ref}}(t)$. However, since both the state eqation (37) and the output equation (41) are non-linear, it is difficult to derive the inverse system and to calculate the input from the output. In section III-B, the method to calculate the inverse system approximately with an offline calculation [11].

B. High-gain feedback and approximate inversion

Fig. 5 is the block diagram of a high gain feedback and approximate inversion. $\boldsymbol{P}$ is the actual plant and $\boldsymbol{P_n}$ is the nominal plant derived by the envelope modeling. K is a constant gain.

If the gain K is large enough, $\boldsymbol{u}(t)$ is generated to satisfy the following equations :

$$\boldsymbol{y}(t) \simeq \boldsymbol{y_{ref}}(t). \tag{42}$$

A proof of (42) is given in this section.

Fig. 5 shows that

$$\boldsymbol{u} = K\left(\boldsymbol{y_{ref}} - \boldsymbol{z}\right) = K\left\{\boldsymbol{y_{ref}} - \boldsymbol{P_n}(\boldsymbol{u})\right\} \tag{43}$$

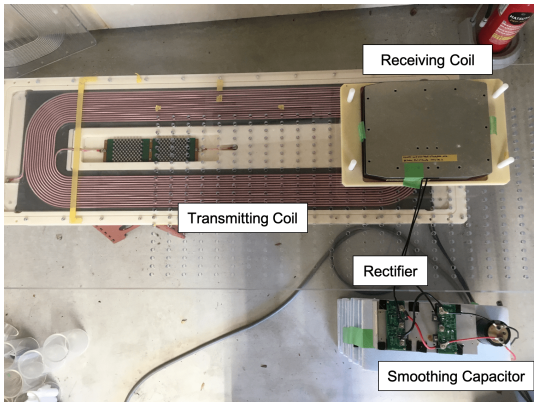

(a) Coils and rectifier

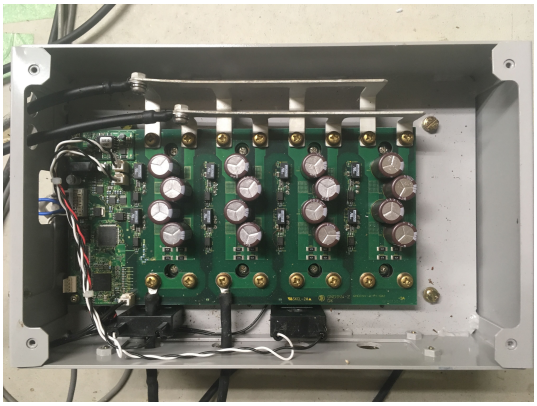

(b) Inverter

Fig. 6. Experimental setup.

TABLE I
PARAMETERS IN THE EXPERIMENT

Parameter	Value
Operating frequency f_0	88.19 kHz
Transmitter inductance L_1	429.0 µH
Transmitter resistance R_1	342.5 mΩ
Receiver inductance L_2	377.7 µH
Receiver resistance R_2	429.0 mΩ
Coupling coefficient k	0.035
Transmitting-side DC-link voltage E_1	100 V
Final value of the amplitude of transmitting-side current $I_{1,max}$	8.48 A
Receiving-side DC-link voltage E_2	50 V
Capacitance of Smoothing capacitor C_f	4700 µF
Control period of transmitting-side inverter	100 µs

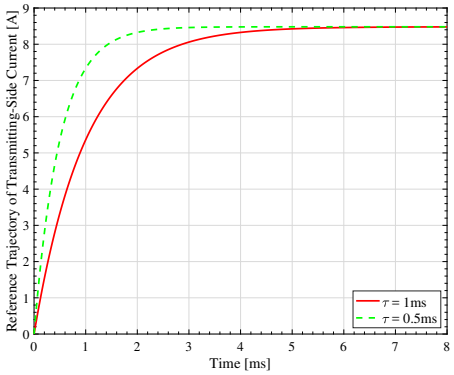

Fig. 7. Reference trajectory of the amplitude of the transmitting-side current $i_{1,ref}$. The time constant of the first-order delay is changed in two conditions.

is true, so

$$K^{-1}\boldsymbol{u} = \boldsymbol{y_{ref}} - \boldsymbol{P_n}(\boldsymbol{u}) \tag{44}$$

$$\Leftrightarrow \boldsymbol{u} = \boldsymbol{P_n}^{-1}\left(\boldsymbol{y_{ref}} - K^{-1}\boldsymbol{u}\right) \tag{45}$$

holds. If K is large enough, an approximation

$$\boldsymbol{u} = \boldsymbol{P_n}^{-1}\left(\boldsymbol{y_{ref}} - K^{-1}\boldsymbol{u}\right) \simeq \boldsymbol{P_n}^{-1}(\boldsymbol{y_{ref}}) \tag{46}$$

is valid and the inverse system of nominal plant $\boldsymbol{P_n}^{-1}$ is obtained by the feedback loop in the left half of Fig. 5. If the envelope modeling is accurate, $\boldsymbol{P} \simeq \boldsymbol{P_n}$ holds. Therefore, (42) is proven.

IV. EXPERIMENT

The authors conducted an experiment in order to verify the availability of the proposed method. Fig. 6 shows the experimental setup. The transmitting coil was connected to the inverter and the transmitting-side voltage can be manipulated by three-level drive, which modulates the timing of ON and OFF of each switch and the AC voltage controllable. The receiving-side coil was connected to the constant voltage load through the diode bridge rectifier. The smoothing capacitor was inserted in parallel with CVL. Circuit parameters are indicated in TABLE I.

The experiment was conducted under three conditions in total : one in the conventional method and two in the proposed method. As the conventional method, the amplitude of the transmitting-side voltage is raised stepwisely. As the proposed methods, the amplitude of the transmitting-side voltage is raised according to the trajectory calculated from the proposed envelope model. MATLAB Simulink was used for the high-gain feedback calculation. Non-linear calculation takes too much time to simulate, so the calculation was conducted by linearized model around operating points.

In order to eliminate the overshoot which occurred when the charging begins, the reference waveform of the amplitude of transmitting-side current $|i_1|$ in the proposed method was a first-order time delay response as shown in Fig. 7. The time constant τ is varied in two conditions : 1 ms and 0.5 ms.

Fig. 8 is the input voltage trajectory and Fig. 9 shows the result of the experiment. In the conventional method, 29 % of overshoot came into being in the transmitting-side current due to the sudden change of the transmitting-side voltage. In the proposed methods, on the other hand, the current tracked the reference trajectory and the overshoot disappeared. The difference in the steady-state values of the proposed methods are thought to be caused by the forward voltage of diodes.

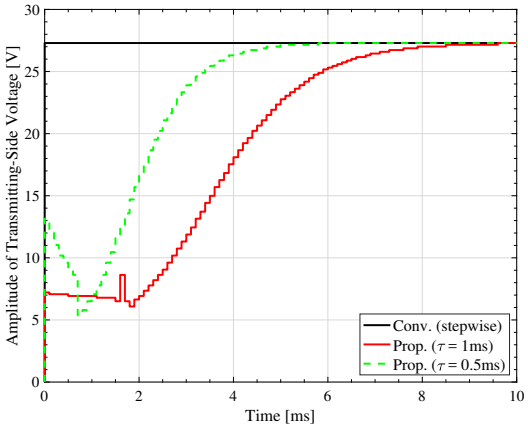

Fig. 8. Input voltage waveforms of each method.

V. Conclusion

In this paper, a novel method of improving the transient response in in-motion WPT by the precise envelope model of circuit was proposed. The discontinuous current mode of diodes was considered and the modeling in [10] was extended. By combining the envelope model into approximate inversion, the method of raising the transmitting-side voltage which does not produce current overshoot was proposed. The proposed method bases on accurate circuit parameters and does not have robustness toward the change of each parameter. Therefore, a control method robust to parameter variations should be discussed as a future work.

Acknowledgment

The authors would like to thank Dr. G. Guidi, a researcher of SINTEF, for useful discussions about the modeling. The contributions of Toyo Denki Seizo K.K. and NSK Ltd. are gratefully acknowledged.

This work was partly supported by JSPS KAKENHI Grant Number 18H03768, JST CREST Grant Number JPMJCR15K3, and JST-Mirai Program Grant Number JPMJMI17EM, and the EIG CONCERT-Japan 4th Call under the Strategic international Research cooperative Program of JST, Japan.

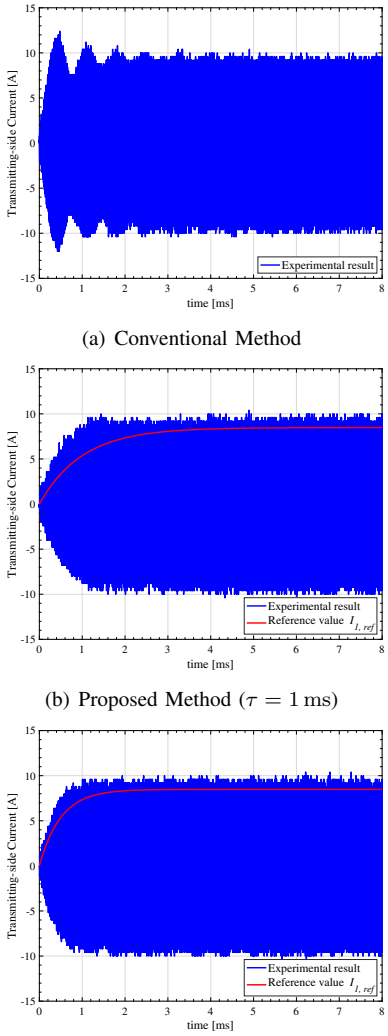

(a) Conventional Method

(b) Proposed Method ($\tau = 1\,\mathrm{ms}$)

(c) Proposed Method ($\tau = 0.5\,\mathrm{ms}$)

Fig. 9. Experimental results of transmitting-side current.

References

[1] A. Kurs, A. Karalis, R. Moffatt, J. D. Joannopoulos, P. Fisher, and M. Soljacic, "Wireless Power Transfer via Strongly Coupled Magnetic Resonances," *Science*, vol. 317, no. 5834, pp. 83–86, jul 2007.

[2] G. Lovison, D. Kobayashi, M. Sato, T. Imura, and Y. Hori, "Secondary-side-only Control for High Efficiency and Desired Power with Two Converters in Wireless Power Transfer Systems," *IEEJ Journal of Industry Applications*, vol. 6, no. 6, pp. 473–481, 2017.

[3] V.-D. Doan, H. Fujimoto, T. Koseki, T. Yasuda, H. Kishi, and T. Fujita, "Simultaneous Optimization of Speed Profile and Allocation of Wireless Power Transfer System for Autonomous Driving Electric Vehicles," *IEEJ Journal of Industry Applications*, vol. 7, no. 2, pp. 189–201, 2018.

[4] D. Patil, M. K. McDonough, J. M. Miller, B. Fahimi, and P. T. Balsara, "Wireless Power Transfer for Vehicular Applications: Overview and Challenges," *IEEE Transactions on Transportation Electrification*, vol. 4, no. 1, pp. 3–37, 2017.

[5] S. Li and C. Mi, "Wireless Power Transfer for Electric Vehicle Applications," *IEEE Journal of Emerging and Selected Topics in Power Electronics*, vol. PP, no. 99, p. 1, 2014.

[6] G. Guidi and J. A. Suul, "Transient Control of Dynamic Inductive EV Charging and Impact on Energy Efficiency when Passing a Roadside Coil Section," in *2018 IEEE PELS Workshop on Emerging Technologies: Wireless Power Transfer (WoW)*. IEEE, jun 2018, pp. 1–7.

[7] K. Hata, T. Imura, H. Fujimoto, and Y. Hori, "Comparison of Soft-Starting Methods for In-Motion Charging of Electric Vehicles to Suppress Start-up Current Overshoot in Wireless Power Transfer System," in *2018 IEEE Transportation Electrification Conference and Expo, Asia-Pacific (ITEC Asia-Pacific)*. IEEE, jun 2018, pp. 1–5.

[8] Y. Guo, L. Wang, Q. Zhu, C. Liao, and F. Li, "Switch-On Modeling and Analysis of Dynamic Wireless Charging System Used for Electric Vehicles," *IEEE Transactions on Industrial Electronics*, vol. 63, no. 10, pp. 6568–6579, oct 2016.

[9] A. Ong, P. K. S. Jayathurathnage, J. H. Cheong, and W. L. Goh, "Transmitter Pulsation Control for Dynamic Wireless Power Transfer Systems," *IEEE Transactions on Transportation Electrification*, vol. 3, no. 2, pp. 418–426, jun 2017.

[10] G. Guidi and J. A. Suul, "Modelling techniques for designing high-performance on-road dynamic charging systems for electric vehicles," in *EVS 31 & EVTeC 2018*, 2018, pp. 1–7.

[11] G. C. Goodwin, S. F. Graebe, and M. E. Salgado, *Control System Design*, 2000.